A novel small-molecule inhibitor reveals a possible role of kinesin-5 in anastral spindle-pole assembly

Aaron C. Groen[1,2,*], Daniel Needleman[1,2], Clifford Brangwynne[2], Christain Gradinaru[2], Brandon Fowler[3], Ralph Mazitschek[3] and Timothy J. Mitchison[1,2]

[1]Harvard Medical School, Department of Systems Biology, 200 Longwood Avenue, WAB536, Boston, MA 02115, USA
[2]Marine Biological Laboratory, 7 MBL Street, Woods Hole, MA 02543, USA
[3]Broad Institute of MIT and Harvard, 7 Cambridge Center, Cambridge, MA 02142, USA
*Author for correspondence (e-mail: aaron_groen@student.hms.harvard.edu)

Accepted 22 April 2008
Journal of Cell Science 121, 2293-2300 Published by The Company of Biologists 2008
doi:10.1242/jcs.024018

Summary

The tetrameric plus-end-directed motor, kinesin-5, is essential for bipolar spindle assembly. Small-molecule inhibitors of kinesin-5 have been important tools for investigating its function, and some are currently under evaluation as anti-cancer drugs. Most inhibitors reported to date are 'non-competitive' and bind to a specific site on the motor head, trapping the motor in an ADP-bound state in which it has a weak but non-zero affinity for microtubules. Here, we used a novel ATP-competitive inhibitor, FCPT, developed at Merck (USA). We found that it induced tight binding of kinesin-5 onto microtubules in vitro. Using *Xenopus* egg-extract spindles, we found that FCPT not only blocked poleward microtubule sliding but also selectively induced loss of microtubules at the poles of bipolar spindles (and not asters or monoasters). We also found that the spindle-pole proteins TPX2 and γ-tubulin became redistributed to the spindle equator, suggesting that proper kinesin-5 function is required for pole assembly.

Supplementary material available online at
http://jcs.biologists.org/cgi/content/full/121/14/2293/DC1

Key words: Kinesin-5, Mitosis, Small-molecule inhibitor, *Xenopus*-extract spindles

Introduction

Bipolar mitotic spindles composed of microtubules, motors and other factors are required for chromosome segregation (McDonald et al., 1979; McIntosh and Euteneuer, 1984; Salmon and Begg, 1980). In most spindles, a plus-end-directed tetrameric motor from the kinesin-5 family (called Eg5 in *Xenopus*) is essential for spindle bipolarity (Cole et al., 1994; Heck et al., 1993; Kapitein et al., 2005; Sawin et al., 1992; Walczak et al., 1998). Kinesin-5 is proposed to function by sliding anti-parallel microtubules apart (Sharp et al., 1999). In spindles from *Xenopus* egg extract, it is also proposed to drive continuous, poleward microtubule sliding during the metaphase steady state (Kapitein et al., 2005; Miyamoto et al., 2004).

An important sub-question for understanding spindle assembly is how spindle poles assemble, particularly in anastral spindles, which lack pre-existing microtubule-nucleating centers. Previous work has shown that kinesin-5 has a role in organizing anastral spindle poles, because poles assembled without kinesin-5 appear as asters with large holes ('holey asters') (Gaglio et al., 1996; Sawin et al., 1992; Sawin and Mitchison, 1994). However, analysis of such disorganized structures is complicated, making further conclusions about how kinesin-5 focuses microtubules into a spindle pole difficult.

Here, we used a novel ATP-competitive inhibitor of kinesin-5, compound-3, also known as 2-[1-(4-fluorophenyl)cyclopropyl]-4-(pyridin-4-yl)thiazole and which we will refer to hereafter as FCPT (Rickert et al., 2008). We found that FCPT induced a tight binding of kinesin-5 onto microtubules and induced loss of microtubules selectively at the poles of *Xenopus*-extract spindles without altering microtubule dynamics. We also found that FCPT blocked poleward microtubule sliding and redistributed the spindle-pole proteins TPX2 and γ-tubulin. Our data suggest that kinesin-5 might have a role in pole assembly in bipolar spindles by either directly or indirectly maintaining microtubule assembly.

Results

Numerous small-molecule kinesin-5 inhibitors have been described and, to date, all act by inhibiting the release of the ADP product (Cochran and Gilbert, 2005; Maliga et al., 2002). Members of this class are called 'non-competitive inhibitors' and induce the formation of monoaster spindles in dividing cells. In this study, we used a representative non-competitive inhibitor, S-trityl-L-cysteine (STLC, see Fig. 1A) (DeBonis et al., 2004), and a novel kinesin-5 inhibitor, FCPT, developed at Merck, that competes with the ATP substrate (Luo et al., 2007; Rickert et al., 2008) (Fig. 1A).

FCPT promoted binding of kinesin-5 to microtubules

FCPT showed good to excellent specificity for kinesin-5 inhibition compared with a panel of eight kinesins and 36 kinases, suggesting that it was suitable for cell biological experiments probing kinesin-5 function (Rickert et al., 2008). Inhibition of the microtubule-stimulated ATPase activity of the kinesin-5 motor domain by FCPT was competitive with the ATP substrate (Rickert et al., 2008), unlike non-competitive inhibitors (Maliga et al., 2002; Cochran et al., 2004). The inhibitor constant (*Ki*) for inhibition of ATPase activity was 110 nM (Rickert et al., 2008).

To test the effect of FCPT on the interaction between kinesin-5 and microtubules, we expressed monomeric motor domain and performed co-sedimentation assays with microtubules. AMP-PNP was used as a control known to promote tight microtubule binding. We found that both FCPT [half-maximal inhibition (EC_{50}) ~65±10 μM] and AMP-PNP (EC_{50} ~116±17 μM) promoted a dose-

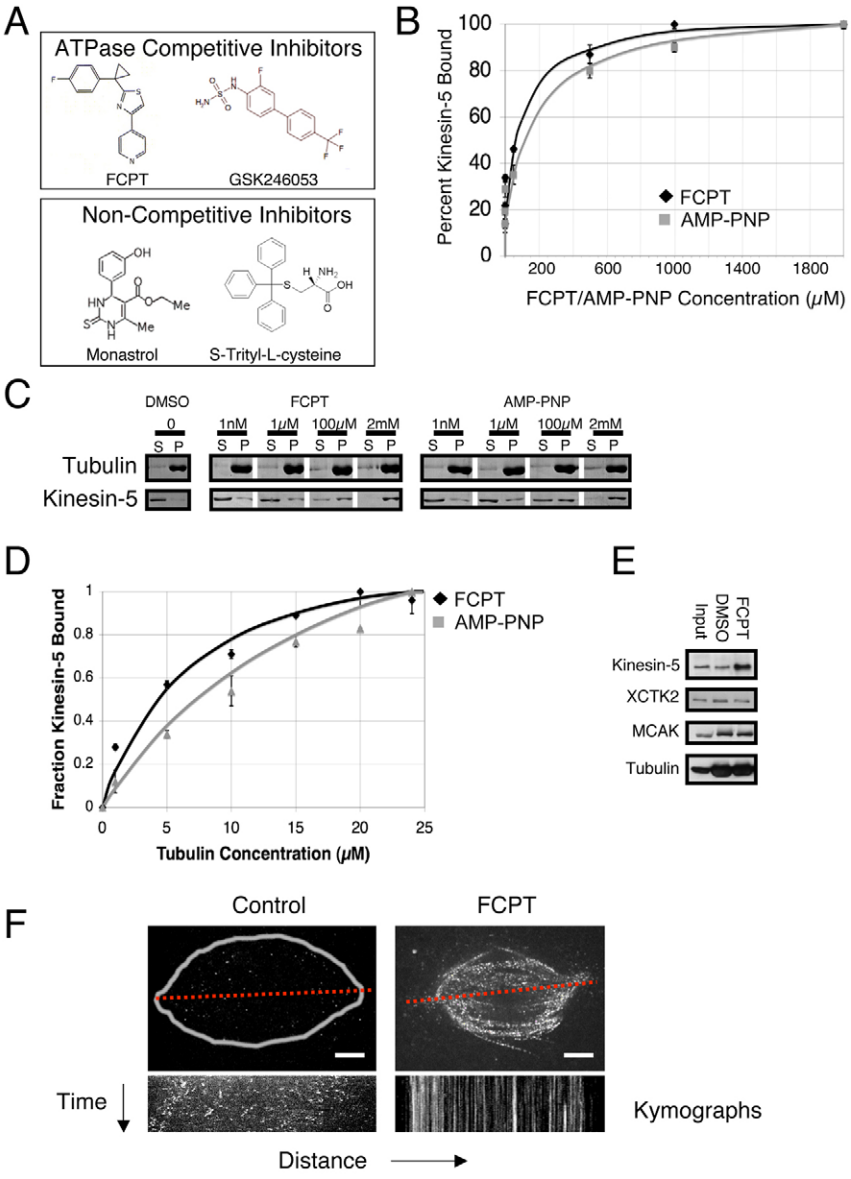

Fig. 1. FCPT induced tight binding of Eg5 to microtubules. (A) The structures of kinesin-5 inhibitors: 2-[1-(4-fluorophenyl)cyclopropyl]-4-(pyridin-4-yl)thiazole (FCPT), GSK246053, monastrol and S-Trityl-L-cysteine (STLC). (B) FCPT, similar to AMP-PNP, induced the binding of the recombinant kinesin-5 motor domain to microtubules (10 μM) in the presence of 1 mM ATP. The best-fit line of the dose-response curve identified the EC_{50} of AMP-PNP as 116 μM (±17 μM) and FCPT as 65 μM (±10 μM). Note that the concentration of FCPT required to bind 100% of the kinesin-5 motor domain to microtubules (1-2 mM) was above the solubility concentration for FCPT (approximately 500-600 μM). Error bars, s.e.m. (C) Coomassie-stained gels of lysates isolated from supernatants (S) and pellets (P) of either a DMSO (control)-, FCPT- or AMP-PNP-treated kinesin-5 motor domain/microtubule mix (in the presence of 1 mM ATP), showing kinesin-5 and tubulin. (D) FCPT enhanced the binding of kinesin-5 to microtubules. The best-fit line identified the apparent K_d of AMP-PNP (grey line) as 6.3 μM (±1.96 μM) and FCPT (black line) as 1.7 μM (±0.437 μM) – both in the presence of 1 mM ATP, 8 μM kinesin-5 and either 10 μM FCPT or 10 μM AMP-PNP. The fraction of kinesin-5 co-sedimenting with microtubules is scaled to reflect maximum binding as 1.0. Error bars, s.e.m. (E) Immunoblots show that FCPT (compared with DMSO as a control) enhanced the binding of kinesin-5 onto pelleted taxol-polymerized microtubules in clarified *Xenopus* egg extracts (approximately threefold); binding of either XCTK2 or MCAK to microtubules was unaffected. Tubulin is a loading control. (F) FCPT inhibited kinesin-5 motility on *Xenopus* egg-extract spindles. The kymographs (measured from the red broken line) of image sequences taken over 3.5 minutes (with one image every 3 seconds) show that X-rhodamine-labeled kinesin-5 is not motile when FCPT (right; 200 μM) was present (shown as straight lines). In the control (left; same time frame as the FCPT condition), kinesin-5 was dynamic, with speckles appearing and disappearing over time. The spindle is outlined with a white line. Scale bars: 5 μm.

dependent increase in the amount of motor domain co-sedimenting with microtubules, whereas very little motor domain co-sedimented in the presence of 1 mM ATP and no drug (Fig. 1B,C).

To calculate the apparent dissociation constant (K_d), we performed co-sedimentation assays with varying concentrations of microtubules (Fig. 1D). Whereas the non-competitive inhibitors reduced the affinity of kinesin-5 for microtubules in the absence of ATP (K_d without inhibitor = 0.7 μM compared with K_d with inhibitor = 2.3 μM), we found that FCPT only enhanced binding in the presence of ATP (data not shown), suggesting that an aspect of the ATPase cycle is important for the activity of FCPT (Cochran et al., 2005). Co-sedimentation of microtubules and kinesin-5 required either FCPT (apparent K_d = 1.7±0.437 μM) or AMP-PNP (apparent K_d = 6.3±1.96 μM); very little kinsin-5 co-sedimented without drug (or AMP-PNP). Unlike AMP-PNP, the activity of FCPT was reversible upon resuspension of the microtubule pellet without drug (data not shown). These experiments show that FCPT, similar to AMP-PNP, locks the motor into a conformation with an increased affinity for microtubules. We will refer to this as 'tight binding'.

To test the efficacy and specificity of the tight-binding effect in cytoplasm, we added taxol to clarified *Xenopus* egg extract with or without FCPT, pelleted the assembled microtubule asters and immunoblotted the pellets for motors involved in spindle morphogenesis. FCPT enhanced recruitment of kinesin-5 (by approximately threefold), whereas recruitment of MCAK, XCTK2, and dynein-dynactin was not affected (Fig. 1E; data not shown).

To test whether FCPT promoted tight binding of kinesin-5 to microtubules in spindles, we added small amounts (approximately 1 μM) of full-length kinesin-5 labeled on random lysines with rhodamine [prepared as in Kapoor and Mitchison (Kapoor and Mitchison, 2001)] to pre-assembled *Xenopus*-extract spindles and imaged the resulting kinesin-5 speckles by spinning-disc confocal microscopy. Without drug, the motor became transiently immobilized, as evidenced by short lines at various angles in the kymograph (Fig. 1F, control). Addition of FCPT (at 200 μM) greatly increased the recruitment of X-rhodamine-labeled kinesin-5 to spindles as quickly as we could assay (less than 2 minutes), and

also caused the speckles to become immobilized for many seconds, as evidenced by the bright, vertical lines in the kymograph (Fig. 1F, FCPT). Thus, the drug also promoted tight binding in the context of assembled spindles. These data also suggest that poleward microtubule sliding is blocked, a point we confirm below with tubulin imaging.

FCPT altered spindle morphology while maintaining bipolarity

FCPT and the non-competitive inhibitors of kinesin-5 each have dramatic but different effects on spindle morphology in meiotic *Xenopus* egg extracts. As previously studied, non-competitive kinesin-5 inhibitors, such as STLC, induced the formation of monoaster spindles in dividing cells (Brier et al., 2004; Mayer et al., 1999; Mitchison et al., 2005). Similar to other non-competitive kinesin-5 inhibitors, we found that STLC addition caused pre-formed *Xenopus* egg-extract spindles to collapse into monoasters over the course of 20 minutes, changing the average pole-pole length from 35 µm to approximately zero (using labeled anti-NuMA IgG to mark the poles; Fig. 2A,B) (Kapoor et al., 2000). The EC_{50} for STLC in this experiment was ~2 µM (concentration of STLC required to assemble 50% monoasters), making it ~20 times more potent than the inhibitor monastrol (Brier et al., 2004; DeBonis et al., 2004).

FCPT addition to assembled spindles caused tubulin fluorescence near the spindle pole to decrease, over ~5 minutes, until ~50% of the initial amount remained (Fig. 2A,C), suggesting a decrease in microtubule density near spindle poles. Tubulin fluorescence near the equator remained approximately constant and, unlike with STLC addition, the pole-pole distance was not changed (Fig. 2B). Despite the decrease in microtubule density at the poles, some pole structure remained, as evidenced by largely unchanged levels of anti-NuMA (Fig. 2A). The EC_{50} of FCPT (concentration required to reduce the ratio of pole:equator fluorescence to approximately 0.8 or 50% of the maximum reduction) for promoting morphological change was ~75 µM, and we used the compound at 200 µM in most experiments. This EC_{50} was higher than that for inducing tight binding with pure proteins, which is typical for hydrophobic drugs in extract, perhaps because much of the drug partitions into lipids. These data from fixed samples were confirmed by time-lapse imaging of drug-treated spindles and the morphological effects observed using labeled tubulin alone were identical in the absence of the anti-NuMA pole marker (data not shown).

The addition of FCPT before spindle assembly induced different morphological changes. Whereas STLC addition, whether added before or after spindle assembly, induced the formation of monoaster spindles, FCPT inhibited spindle assembly and produced structures with disorganized, elongated microtubules (Fig. 2D; data not shown). Thus, consistent with its role in perturbing an essential meiotic kinesin, such as kinesin-5, FCPT affects spindle morphology whether added before or after spindle assembly.

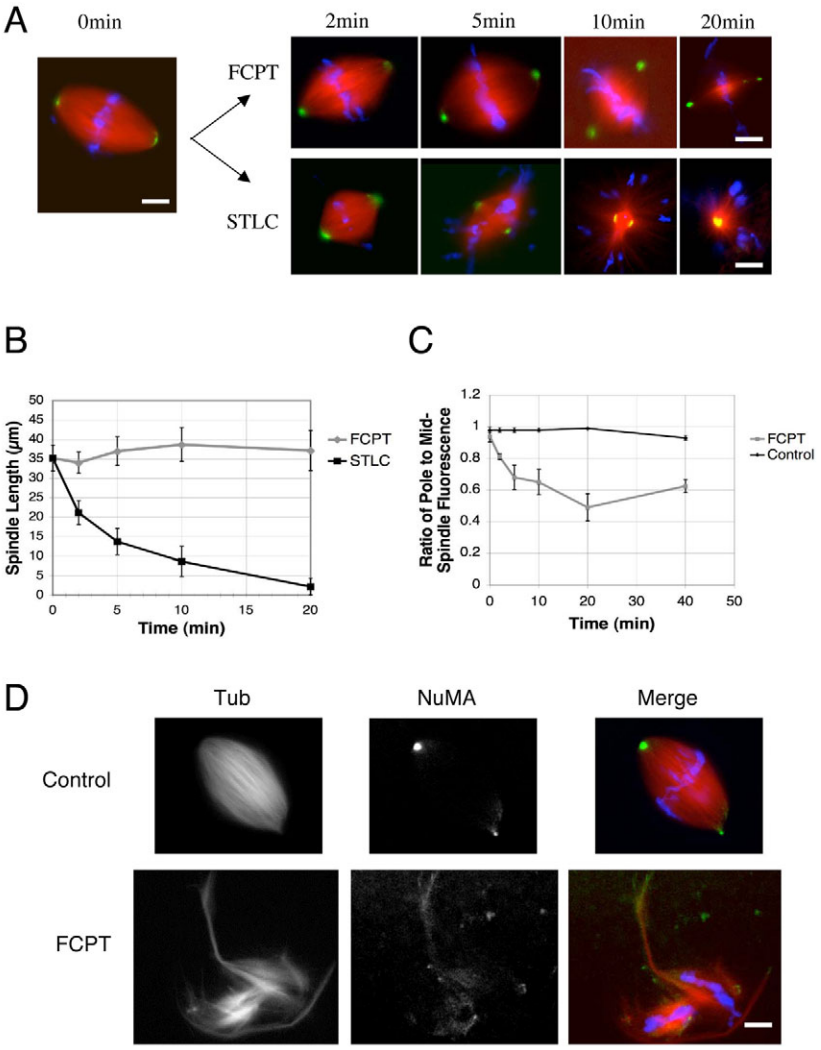

Fig. 2. FCPT decreased spindle-pole microtubule density. (A) FCPT-treated (200 µM) *Xenopus* egg-extract spindles did not collapse, whereas STLC (non-competitive kinesin-5 inhibitor)-treated spindles collapsed within 20 minutes. Fixed images of different spindles at time points up to 20 minutes showing tubulin (red), NuMA (green) and DNA (blue) are shown. The spindle-pole marker NuMA remained localized to the spindle pole in the presence of FCPT. (B) FCPT-treated *Xenopus* egg-extract spindles maintained a constant length of about 35 µm, whereas STLC-treated spindles collapsed to approximately 0 µm over 20 minutes. Error bars, s.e.m.; n=6 for each time point. (C) The ratio of the fluorescence of the spindle-poles:mid-spindle decreased from approximately 0.9 to approximately 0.6 over 40 minutes. Error bars, s.e.m.; n=6 for each time point. (D) Spindles assembled in the presence of FCPT are elongated and asymmetric, compared with controls, which are bipolar. Fixed images of spindles showing tubulin (red), NuMA (green) and DNA (blue) are shown. NuMA was diffusely localized on FCPT-treated spindles. Scale bars: 10 µm.

FCPT altered spindle-pole composition of bipolar spindles

We found that FCPT lowered microtubule density at spindle poles of bipolar spindles (Fig. 2). To test whether FCPT also affects the protein composition of spindle poles, we measured the effect of FCPT on the localization of the spindle-pole markers TPX2 and γ-tubulin. Each is required for assembly of microtubules during spindle assembly in extract (Gruss et al., 2001; Zheng et al., 1995). To visualize TPX2 and γ-tubulin, we used a TPX2-GFP fusion protein and a non-perturbing, labeled anti-γ-tubulin antibody (Fig. 3A,B). FCPT caused TPX2 and γ-tubulin to relocalize from the poles to the band of remaining microtubules at the equator. The

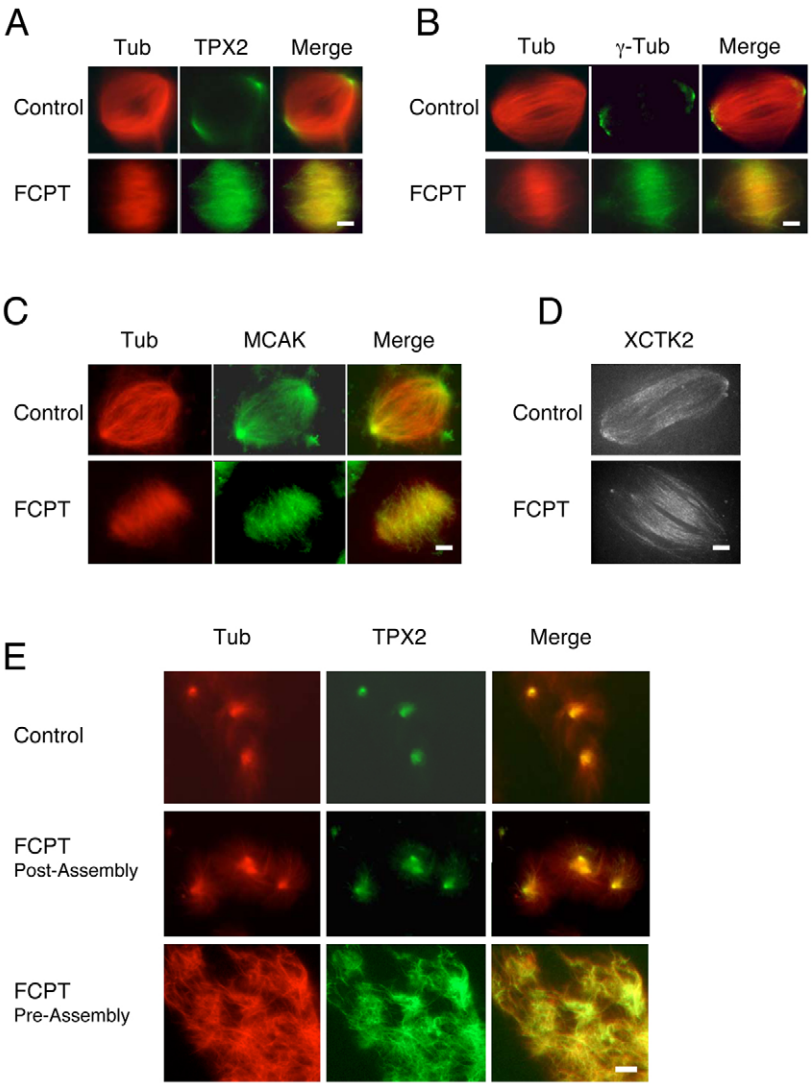

Fig. 3. FCPT redistributed TPX2 and γ-tubulin from the spindle pole of bipolar spindles. (A-D) Fixed images of spindles treated with (and without) FCPT for approximately 20 minutes: tubulin (red), TPX2 (A; green), γ-tubulin (B; green), MCAK (C; green), XCTK2 (D). (A,B) FCPT redistributed the localizations of TPX2 and γ-tubulin from the spindle pole to the equator of the mid-spindle. (C,D) FCPT removed the localization of MCAK and XCTK2 from the spindle pole. (E) Fixed images of FCPT-treated DMSO asters after (FCPT post-assembly) and before (FCPT pre-assembly) aster assembly: tubulin (red) and TPX2 (green). FCPT addition after DMSO aster formation (FCPT post-assembly) had no effect on the aster pole and localization of TPX2, whereas FCPT treatment before aster formation (FCPT pre-assembly) perturbed aster pole assembly and the pole localization of TPX2. Scale bars: 10 μm.

redistributions occurred over the same time scale as the microtubule loss at the spindle poles (data not shown; Fig. 2). Additionally, the kinesins XCTK2 and MCAK also disappeared from the FCPT-treated spindle poles (at the same rate as tubulin) but, unlike TPX2 and γ-tubulin, neither were significantly enhanced in the spindle equator (Fig. 3C,D). We also found that FCPT did not enhance the binding of either TPX2, γ-tubulin, XCTK2 or MCAK to microtubules, as shown by western blot analysis of taxol-polymerized microtubule pellets isolated from extracts (Fig. 1E; supplementary material Fig. S1A). Thus, FCPT might perturb the protein composition of intact poles of bipolar spindles by either affecting microtubule dynamics (transport, polymerization or depolymerization) or directly changing the recruitment of spindle-pole factors.

Aster poles did not undergo FCPT-dependent morphological changes

To better understand the effect that FCPT has on spindle poles, we added FCPT to microtubule asters. We induced the formation of microtubules in extracts with DMSO, which assembled into aster-like structures after 30 minutes (Fig. 3E). As shown previously, such structures localized NuMA, TPX2 and γ-tubulin (Groen et al., 2004; Wittmann et al., 1998; Wittmann et al., 2000). Similar to bipolar spindles, we found that the addition of FCPT to preformed asters induced the recruitment and immobilization of kinesin-5 to the aster (data not shown). FCPT addition before aster assembly abolished the assembly of all organized structures and mislocalized the pole markers TPX2 and NuMA (Fig. 3E; supplementary material Fig. S2A). However, surprisingly, unlike bipolar spindles, we found that the addition of FCPT after aster assembly did not affect the aster structure and pole (Fig. 3E). We found that the localization of pole markers such as NuMA, TPX2 and γ-tubulin were also not drastically changed (Fig. 3E; supplementary material Fig. S2A; data not shown). Similar effects were observed for RanGTP-induced asters or STLC-induced monoasters (supplementary material Fig. S2B; data not shown). Our data suggest that FCPT requires bipolarity (anti-parallel microtubules) to influence spindle-pole structure.

Effect of FCPT on microtubule dynamics

Microtubules in extract spindles undergo poleward sliding, driven at least in part by kinesin-5 (Miyamoto et al., 2004). Non-competitive kinesin-5 inhibitors inhibit poleward sliding, so we wanted to test whether FCPT had similar effects. FCPT caused a dose-dependent decrease of the poleward microtubule-sliding rate, measured by tubulin speckle imaging (Sawin and Mitchison, 1991; Waterman-Storer et al., 1998), with an EC_{50} of ~30 μM (Fig. 4A,B). Similar to the recruitment of rhodamine-labeled kinesin-5 to spindles, the inhibition of poleward sliding occurred as fast as we could assay (less than 2 minutes), suggesting that the inhibition of poleward sliding is most probably due to perturbation of kinesin-5.

To determine the role that FCPT had in microtubule polymerization at the spindle pole, we imaged labeled Alexa-Fluor-488-conjugated EB1 – a marker of microtubule polymerization – on control and FCPT-treated spindles (Tirnauer et al., 2002b; Tirnauer et al., 2004). On control spindles, as shown previously, EB1 localized throughout the spindle, tracking along growing microtubule tips, suggesting that polymerization occurs throughout the spindle (Tirnauer et al., 2002a). In FCPT-treated spindles, EB1 disappeared from the spindle pole over a similar time scale as the microtubule loss at the spindle poles (approximately 5 minutes) and remained localized to the band of microtubules at the equator with no significant change in overall tip-tracking dynamics in this region

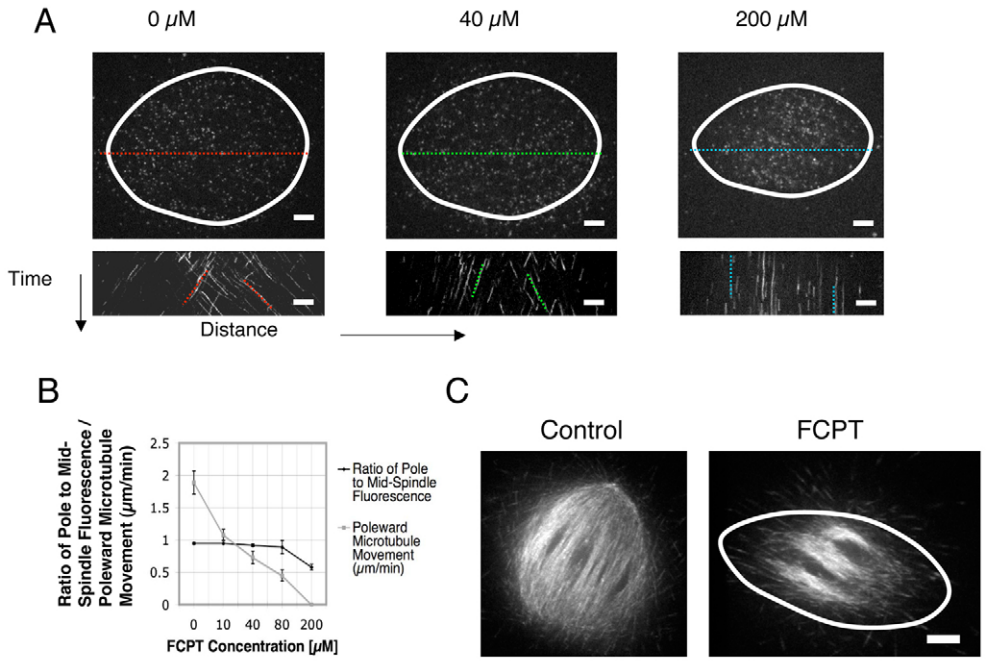

Fig. 4. FCPT inhibited poleward microtubule movement and spindle-pole polymerization. (A) FCPT inhibition of poleward microtubule movement was titratable. Localizations of speckle level Alexa-Fluor-647-conjugated tubulin on *Xenopus* egg-extract spindles with 0, 40 and 200 μM FCPT. The kymographs (measured from colored broken lines) of image sequences obtained over the course of approximately 3.5 minutes (with one image every 3 seconds) show that poleward movement is only inhibited upon addition of 200 μM FCPT. Intermediate concentrations of FCPT had intermediate microtubule poleward rates (see B). Untreated control spindles had a microtubule poleward movement of approximately 1.9 ± 0.2 μm/minute (± s.e.m.). The spindle is outlined with a white line. Scale bar: 5 μm. (B) The reduction of spindle-pole density (as measured by the ratio of spindle-pole:mid-spindle fluorescence) only occurred at FCPT concentrations sufficient to completely inhibit poleward microtubule movement (200 μM). Error bars, s.e.m.; n=3 for each point. (C) Alexa-Fluor-488-EB1 localized on control and FCPT-treated spindles. FCPT removed spindle-pole localization of EB1 compared with controls (imaged approximately 4-5 minutes after FCPT addition; The spindle is outlined with a white line). See supplementary material Movies 1, 2. Scale bar: 10 μm.

(Fig. 4C; supplementary material Movies 1, 2; data not shown). Thus, FCPT locally inhibits microtubule polymerization at the spindle pole of a bipole, but does not directly affect microtubule polymerization elsewhere.

Specificity of FCPT effects

We found that the EC_{50} for poleward-sliding inhibition (30 μM) was lower than that for the morphological changes at spindle poles (~75 μM; Fig. 2; Fig. 4B), suggesting the possibility of two targets with different binding affinities for FCPT. Although we cannot rule out this possibility, there are also many other equally possible explanations. For example, microtubule assembly (and/or the transport of assembly factors) might depend on poleward microtubule sliding and therefore the loss of microtubule assembly at the spindle pole might only occur when sliding is inhibited above a particular threshold, leading to a higher EC_{50} for the morphological changes. Consistent with this model, we found that the FCPT-dependent inhibition of poleward sliding always occur (temporally) before the morphological changes at the spindle pole. Further experiments should address these models.

To further evaluate the specificity of the effects of FCPT on *Xenopus*-extract spindles, we tested a structurally dissimilar compound that might act by a similar mechanism. Biphenyl sulfamide 20 [referred to here as GSK246053 (Fig. 1A)] was developed as a specific ATPase-competitive kinesin-5 inhibitor by Cytokinetics and GlaxoSmithKline (Parrish et al., 2007). Mutations in the non-competitive site of kinesin-5, which block binding of non-competitive inhibitors, had no effect on ATPase inhibition by GSK246053, suggesting that it binds at a novel site (Parrish et al., 2007). GSK246053 had the same effect as FCPT in the co-sedimentation assay in *Xenopus* extract and in all of our spindle assays (supplementary material Fig. S1B-D). This similarity of effects between two structurally unrelated compounds, both developed as specific kinesin-5 inhibitors, provides confidence that our observed gain-of-function phenotypes result from successfully targeting the active site of kinesin-5.

Discussion

Implications for spindle assembly

In this study, we found that an ATP-competitive inhibitor of kinesin-5, FCPT, reversibly binds the motor onto microtubules and produces many gain-of function phenotypes on extract spindles. Interestingly, we found that it lowered spindle-pole microtubule density in bipolar spindles, but not DMSO-induced asters or STLC monoasters. Because asters and monoasters contain fewer anti-parallel microtubules than bipolar spindles (Heald et al., 1997; Kapoor et al., 2000; Mitchison et al., 2004), such experiments suggest that the observed FCPT phenotypes either require anti-parallel microtubules or that the poles of monoasters/asters and bipolar spindles rely on different assembly mechanisms. Further experiments are required to test this hypothesis.

From our data, it is not clear whether the reduction of EB1 at spindle poles reflects spatial changes in microtubule turnover (i.e. increase in catastrophes at spindle poles) or spatial changes in microtubule nucleation (i.e. less microtubule nucleation at spindle poles). The FCPT-dependent loss of microtubule density at spindle

poles could directly result from the inhibition of the transport of microtubules to the pole. Additionally, it could result from the inhibition and/or mislocalization of polymerization factors (such as TPX2 and γ-tubulin) or the activation and/or mislocalization of depolymerization factors (such as Op18 and MCAK). Although we did not observe the FCPT-dependent recruitment of MCAK to the spindle pole (Fig. 3C), there could be other unidentified depolymerization factors recruited to the spindle pole after FCPT treatment. Further experiments need to address these issues.

TPX2, γ-tubulin and NuMA were previously argued to accumulate at poles owing to dynein-dynactin-mediated transport (Buendia et al., 1990; Merdes et al., 1996; Verde et al., 1991; Wittmann et al., 1998), a mechanism that should be insensitive to kinesin-5 perturbation with FCPT. Interestingly, the pole localizations of TPX2 and γ-tubulin were perturbed by FCPT treatment, whereas the localization of NuMA was unaffected, suggesting that TPX2 and γ-tubulin depend upon other mechanisms, such as kinesin-5-dependent poleward sliding, to concentrate on spindle poles. Although perturbation of the dynein-dynactin complex does not inhibit poleward sliding (Maddox et al., 2003), the dynein-dynactin complex has a role in organizing microtubules into poles as well as in transporting materials along them (Merdes et al., 1996; Wittmann and Hyman, 1999). However, distinguishing transport with dynein-dynactin from transport by attachment to sliding microtubules will be difficult, and we suspect that both mechanisms are important. Overall, FCPT is an interesting tool for mitosis research and a testament to the rich pharmacology of motor proteins.

Materials and Methods

Synthesis of FCPT and GSK246053

Synthesis of FCPT was performed with minor modifications according to the procedure reported in Parrish, C. A. and Dhanak, D. (2005). 'Preparation of substituted N-(biphenylyl)sulfamides as kinesin inhibitors for treating cellular proliferative diseases and disorders.' *PCT Int. Appl.* WO 2005062847.

1-(4-fluorophenyl)cyclopropanecarbonitrile

See Fig. 5 for structure. 10.00 g (7.4 mmol) (4-fluorophenyl)-acetonitrile and 9.56 ml (11.1 mmol) 1,2-dibromoethane were dissolved in 60 ml Toluene followed by addition of 2.0 g (7.4 mmol) tetra-N-butylammonium chloride and 60 ml aqueous 12 M sodium hydroxide. The reaction mixture was stirred at room temperature. After 24 hours, 200 ml ethyl acetate was added, and the organic layer was separated and washed twice with water. The combined organic layers were dried over sodium sulfate and the solvent was removed under reduced pressure. The crude product was purified on silica (Hexanes/ethyl acetate 5:1) to yield 5.80 g (49%) of the desired product as yellow oil.

Proton nuclear magnetic resonance (^{1}H NMR) (300 MHz, CDCl3) δ7.30 (m, 2H), 7.06 (t, 2H, J=8.6), 1.73 (q, 2H, J=5.1), 1.38 (q, 2H, J=5.3).

1-(4-fluorophenyl)cyclopropanecarbothioamide

See Fig. 6 for structure. 5.20 g (32.3 mmol) 1-(4-fluorophenyl)-cyclopropane-carbonitrile, 7.22 g (35.5 mmol) magnesium chloride hexahydrate and 10.8 g (19.4 mmol) sodium hydrogen sulfide were dissolved in 100 ml N,N-dimethylformamide (Manaka, 2005). The reaction mixture was heated to 50°C. After 3 hours the reaction mixture was poured into 600 ml water whereby a white precipitate forms. The aqueous layer was extracted three times with ether and the combined organic layers were washed with water. The combined organic layers were dried over sodium sulfate and the solvent was removed under reduced pressure to yield an off-white fluffy solid that was triturated twice with hexanes and dried under reduced pressure to yield 4.80 g of the desired product as white powder.

^{1}H NMR (300 MHz, CDCl3) δ 7.85 (s, 1H), 7.40 (m, 2H), 7.09 (t, 2H, J=8.6), 6.57 (s, 1H), 2.06 (q, 2H, J=3.7), 1.32 (q, 2H, J=3.7).

2-[1-(4-fluorophenyl)cyclopropyl]-4-(pyridin-4-yl)thiazole (FCPT)

See Fig. 1A for structure. 2.0 g (10.2 mmol) 1-(4-fluorophenyl)-cyclopropane-carbothioic acid amide and 2.88 g (10.2 mmol) 2-bromo-1-(pyridin-4-yl)ethanone hydrobromide were suspended in 100 ml ethanol and heated to reflux for 2 hours. Upon cooling, the product precipitated. The precipitate was filtered off, washed with cold ethanol and dried under reduced pressure to yield 2.44 g (63%) of the desired product as hydrobromide (yellow powder) without additional purification.

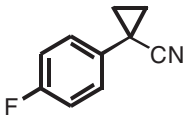

Fig. 5. Structure of 1-(4-fluorophenyl)cyclopropanecarbonitrile.

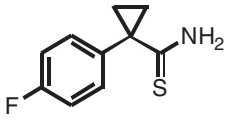

Fig. 6. Structure of 1-(4-fluorophenyl)cyclopropanecarbothioamide.

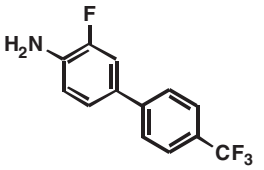

Fig. 7. Structure of 3-fluoro-4′-(trifluoromethyl)biphenyl-4-amine.

^{1}H NMR (300 MHz, CDCl3) δ 8.85 (d, 2H, J=6.4), 8.43 (d, 2H, J=6.4), 8.11 (s, 1H), 7.47 (dd, 2H, J=5.5, 8.3), 7.09 (t, 2H, J=8.6), 1.86 (dd, 2H, J=3.7, 6.3), 1.51 (dd, 1H, J=3.8, 6.4).

Synthesis of GSK246053 was performed with minor modifications according to the procedure reported in Coleman, P. J., Garbaccio, R. M. and Neilson, L. A. (2005). 'Preparation of substituted thiazoles as mitotic kinesin inhibitors.' vol. US2005176776 (ed. U. S. P. A. Publ.). USA.

3-fluoro-4′-(trifluoromethyl)biphenyl-4-amine

See Fig. 7 for structure. A solution of 1.6 g tetrakis triphenylphosphane palladium in 10 ml DMF was added to a solution of 6.61 g (34.8 mmol) 4-(trifluoromethyl)phenyl boronic acid and 5.51 g (29 mmol) 4-bromo-2-fluoro-anilin in 40 ml DMF and 50 ml 2 M aqueous potassium carbonate. The reaction mixture was thoroughly purged with argon and stirred at 100°C for 16 hours. After cooling to room temperature, the reaction mixture was poured in 400 ml of half-saturated aqueous sodium bicarbonate solution and extracted three times with ether. The combined organic layers were dried over sodium sulfate and concentrated under reduced pressure. The crude product was purified on silica (20% ethyl acetate in hexanes) to yield 5.5 g (72%) of the desired product as a white powder.

^{1}H NMR (500 MHz, CDCl3) δ 7.65 (d, 2H, J=8.4), 7.61 (d, 2H, J=8.4), 7.27 (dd, 1H, J=1.8, 12.2), 7.22 (dd, 1H, J=1.8, 8.2), 6.86 (t, 1H, J=8.7), 3.90 (s, 2H).

GSK246053

See Fig. 1A for structure. 149 μl of water was added to a solution of 718 μl (8.25 mmol) chlorosulfonyl isocyanate in 17.5 ml acetonitrile at 0°C. The reaction was stirred for 1 minute at 0°C and for 3 hours at 25°C. After cooling to 0°C, a solution of 1.91 g (7.5 mmol) 3-fluoro-4′-(trifluoromethyl)biphenyl-4-amine in 17.5 ml acetonitrile and 1.25 ml pyridine was added dropwise. The reaction mixture was then warmed to room temperature. After 15 hours, the reaction mixture was diluted with brine and extracted with ethyl acetate. The combined organic layers were dried over sodium sulfate and concentrated under reduced pressure. The crude product was purified on silica gel (35% ethyl acetate in hexanes) to yield 660 mg (26%) of the desired product as white solid.

^{1}H NMR (500 MHz, CDCl3/CD3OD) δ 7.70 (t, 2H, J=7.2), 7.65 (t, 2H, J=8.3), 7.39 (dd, 2H, J=5.7, 17.3), 6.71 (s, 1H).

Xenopus egg-extract spindles

Cycled *Xenopus* egg-extract spindles were assembled from meiotic *Xenopus* egg extracts [cytostatic factor (CSF)] as described previously (Desai et al., 1999; Murray, 1991). Briefly, spindles were assembled from CSF extract containing demembranated sperm nuclei (500/μl) and cycled from interphase (with addition of 0.4 mM $CaCl_2$) for 80 minutes back to meiosis (with addition CSF). After spindle assembly (1-2 hours after CSF addition), spindle reactions were supplemented with various amounts of either FCPT (diluted in DMSO to 200 mM), 200 μM STLC (diluted in DMSO to 100 mM) or 200 μM GSK246053. Tubulin was visualized by the addition of purified bovine tubulin (20 μg/ml) directly labeled with X-rhodamine (Invitrogen) or Alexa

Fluor 647 (Invitrogen) as described previously (Hyman et al., 1991; Sawin and Mitchison, 1991). Generally, experiments were repeated three to six times using three different extracts.

Real-time imaging

Real-time images were obtained using a 100×/1.4 NA Plan Apochromat objective (Nikon) on a Nikon TE 300 inverted microscope fitted with a Yokogawa spinning-disc confocal head (Perkin Elmer) using an Andor EM-CCD camera (512 × 512 pixel sensor) driven by Andor software (Andor).

Real-time images and fixed images were obtained using either a 20×/0.75 NA Plan Apochromat or a 40×/0.95 NA Plan Apochromat objective (Nikon) on an upright Nikon Eclipse 90i using an Orca ER cooled CCD camera (Hamamatsu) driven by Metamorph software (Molecular Devices).

NuMA and γ-tubulin were imaged by addition of 10 μg/ml of Alexa-Fluor-488 (Invitrogen) directly labeled antibodies (Groen et al., 2004) after spindle assembly and FCPT treatment.

Recombinant EB1 was labeled with NHS-ester-Alexa-Fluor-488 (Invitrogen) and imaged by addition of 50 nM to extracts before spindle assembly.

TPX2 was imaged by addition of approximately 20 nM of purified human GFP-TPX2 to extracts before spindle assembly. Human TPX2-GFP was purified from HeLa S3 suspension cells. Briefly, 1 l of cells was transfected using 750 μl Lipofectamine (Invitrogen) with 500 μg of purified pcDNA3.1-GFP-hTPX2 (a kind gift from S. Garrett and T. Kapoor, Rockefeller University). Lysates containing GFP-TPX2 were created by sonicating frozen pellets (created by pelleting and washing suspension cells three times in PBS, 1000 ***g***, 5 minutes each spin, 4°C) in 10× the volume of pellet in XB with no sucrose added (10 mM HEPES, pH 7.7, 100 mM KCl, 1 mM $MgCl_2$, 100 μM $CaCl_2$) supplemented with 1 mM DTT and protease inhibitors (Roche Applied Scientific). The lysates were clarified (50,000 ***g*** for 30 minutes) and GFP-TPX2 was purified first with a 5 ml HiTRAP S column (GE Healthcare) and eluted with XB (no sucrose added) supplemented with 250 mM KCl. The fraction containing GFP-TPX2 was applied to a Superose-12 10/300 gel-filtration column (GE Healthcare) equilibrated with XB + 10% sucrose, 1 mM DTT. GFP-TPX2-containing fractions were frozen in liquid nitrogen.

Microtubule pelleting assay

To determine the FCPT EC_{50} for binding of kinesin-5 to microtubules in vitro, Taxol (Sigma)-stabilized microtubules (10 μM) and 4 μM clarified (200,000 ***g*** for 20 minutes) gel-filtered (Superose-6 10/300 gel) recombinant HIS-kinesin-5 motor domain [amino acids 1-370; a kind gift from S. Kim and E. Wojcik, Louisana State University (Wojcik et al., 2004)] were incubated with varying concentrations of either AMP-PNP, FCPT or DMSO (control) for 5 minutes at room temperature. For the apparent K_d, varying concentrations of taxol-stabilized microtubules were incubated with 8 μM kinesin-5 and 10 μM of either FCPT or AMP-PNP. All samples were pelleted through a 20% glycerol cushion (150,000 ***g*** for 10 minutes). All buffers contained saturating amounts of ATP (1 mM ATP) in 1× BRB-80 plus 10 μM taxol and the appropriate concentration of FCPT. The supernatant and the pellet of each reaction were supplemented with sample buffer for Coomassie-stained SDS-PAGE. The fraction of kinesin-5 co-sedimenting with microtubules was determined using Image Pro (NIH). The best-fit curves (for the apparent K_d and EC_{50} calculations with a 95% confidence) were determined using Igor Pro (Wavemetrics) fitting to the equations: (kinesin-5 fraction bound) = $(c\times x)/(x+EC_{50})$ and (kinesin-5 fraction bound) = $(c\times x)/(x+K_d)$, where x is the concentration of drug for EC_{50} measurements or concentration of tubulin for apparent K_d measurements. A correction constant (c) was necessary to fit each curve.

Taxol (10 μM; Sigma)-induced microtubules from clarified *Xenopus* meiotic egg extracts (crude CSF spun 200,000 ***g***, 2 hours) containing either 200 μM FCPT or DMSO (control) were pelleted (20,000 ***g***, 10 minutes). The pellet was washed three times with 500 μl CSF-XB supplemented with 1 mM ATP, 1 mM GTP, 1 mM DTT, taxol (10 μM) and either 200 μM FCPT or GSK246053. The final pellet was resuspended in 20 μl of sample buffer for use in western blot analysis probing against Eg5, XCTK2, MCAK, TPX2, γ-tubulin and tubulin.

Image analysis

Kymographs were taken from real-time image sequences using lines of 3-μm-width over maximum intensity particles on Metamorph (Molecular Devices). Average flux rates were calculated from manually tracking 10-15 particles on kymographs for three to six spindles from three different extract experiments for each condition.

The images from EB1 movies were aligned with StackReg plugin (Thévenaz et al., 1998).

The ratio of spindle-pole:mid-spindle fluorescence was obtained by taking the average of the integrated intensity at each pole divided by the integrated intensity of the mid-spindle (within 1-3 μm of the chromatin) over a fixed rectangle for each spindle using ImageJ (NIH).

This project began during the 2006 Physiology Course at the Marine Biological Laboratory (MBL) at Woods Hole. We thank Physiology Course students C. Kilburn, C. Hentrich, E. Toprak, M. Bettencourt-Dias, C. Brawley and M. Zuccolo, and all members of the Physiology Course 2006. We also thank T. Maresca, J. Gatlin, C. Field and the MBL Cell Division Group. We thank Andor for loaning the EM-CCD camera (512×512 pixel sensor), and K. Hendricks (Nikon), H. Luther (MBL) and M. Peterson (MBL) for general equipment. We thank Paul Chang (MIT) for advice in TPX2-GFP purifications. T.J.M. was funded by CA078048-09 (National Cancer Institute).

References

Brier, S., Lemaire, D., Debonis, S., Forest, E. and Kozielski, F. (2004). Identification of the protein binding region of S-trityl-L-cysteine, a new potent inhibitor of the mitotic kinesin Eg5. *Biochemistry* **43**, 13072-13082.

Buendia, B., Antony, C., Verde, F., Bornens, M. and Karsenti, E. (1990). A centrosomal antigen localized on intermediate filaments and mitotic spindle poles. *J. Cell Sci.* **97**, 259-271.

Cochran, J. C. and Gilbert, S. P. (2005). ATPase mechanism of Eg5 in the absence of microtubules: insight into microtubule activation and allosteric inhibition by monastrol. *Biochemistry* **44**, 16633-16648.

Cochran, J. C., Sontag, C. A., Maliga, Z., Kapoor, T. M., Correia, J. J. and Gilbert, S. P. (2004). Mechanistic analysis of the mitotic kinesin Eg5. *J. Biol. Chem.* **279**, 38861-38870.

Cochran, J. C., Gatial, J. E., 3rd, Kapoor, T. M. and Gilbert, S. P. (2005). Monastrol inhibition of the mitotic kinesin Eg5. *J. Biol. Chem.* **280**, 12658-12667.

Cole, D. G., Saxton, W. M., Sheehan, K. B. and Scholey, J. M. (1994). A "slow" homotetrameric kinesin-related motor protein purified from Drosophila embryos. *J. Biol. Chem.* **269**, 22913-22916.

DeBonis, S., Skoufias, D. A., Lebeau, L., Lopez, R., Robin, G., Margolis, R. L., Wade, R. H. and Kozielski, F. (2004). In vitro screening for inhibitors of the human mitotic kinesin Eg5 with antimitotic and antitumor activities. *Mol. Cancer Ther.* **3**, 1079-1090.

Desai, A., Murray, A., Mitchison, T. J. and Walczak, C. E. (1999). The use of Xenopus egg extracts to study mitotic spindle assembly and function in vitro. *Methods Cell Biol.* **61**, 385-412.

Gaglio, T., Saredi, A., Bingham, J. B., Hasbani, M. J., Gill, S. R., Schroer, T. A. and Compton, D. A. (1996). Opposing motor activities are required for the organization of the mammalian mitotic spindle pole. *J. Cell Biol.* **135**, 399-414.

Groen, A. C., Cameron, L. A., Coughlin, M., Miyamoto, D. T., Mitchison, T. J. and Ohi, R. (2004). XRHAMM functions in ran-dependent microtubule nucleation and pole formation during anastral spindle assembly. *Curr. Biol.* **14**, 1801-1811.

Gruss, O. J., Carazo-Salas, R. E., Schatz, C. A., Guarguaglini, G., Kast, J., Wilm, M., Le Bot, N., Vernos, I., Karsenti, E. and Mattaj, I. W. (2001). Ran induces spindle assembly by reversing the inhibitory effect of importin alpha on TPX2 activity. *Cell* **104**, 83-93.

Heald, R., Tournebize, R., Habermann, A., Karsenti, E. and Hyman, A. (1997). Spindle assembly in Xenopus egg extracts: respective roles of centrosomes and microtubule self-organization. *J. Cell Biol.* **138**, 615-628.

Heck, M. M., Pereira, A., Pesavento, P., Yannoni, Y., Spradling, A. C. and Goldstein, L. S. (1993). The kinesin-like protein KLP61F is essential for mitosis in Drosophila. *J. Cell Biol.* **123**, 665-679.

Hyman, A., Drechsel, D., Kellogg, D., Salser, S., Sawin, K., Steffen, P., Wordeman, L. and Mitchison, T. (1991). Preparation of modified tubulins. *Meth. Enzymol.* **196**, 478-485.

Kapitein, L. C., Peterman, E. J., Kwok, B. H., Kim, J. H., Kapoor, T. M. and Schmidt, C. F. (2005). The bipolar mitotic kinesin Eg5 moves on both microtubules that it crosslinks. *Nature* **435**, 114-118.

Kapoor, T. M. and Mitchison, T. J. (2001). Eg5 is static in bipolar spindles relative to tubulin: evidence for a static spindle matrix. *J. Cell Biol.* **154**, 1125-1133.

Kapoor, T. M., Mayer, T. U., Coughlin, M. L. and Mitchison, T. J. (2000). Probing spindle assembly mechanisms with monastrol, a small molecule inhibitor of the mitotic kinesin, Eg5. *J. Cell Biol.* **150**, 975-988.

Luo, L., Parrish, C. A., Nevins, N., McNulty, D. E., Chaudhari, A. M., Carson, J. D., Sudakin, V., Shaw, A. N., Lehr, R., Zhao, H. et al. (2007). ATP-competitive inhibitors of the mitotic kinesin KSP that function via an allosteric mechanism. *Nat. Chem. Biol.* **3**, 722-726.

Maddox, P., Straight, A., Coughlin, P., Mitchison, T. J. and Salmon, E. D. (2003). Direct observation of microtubule dynamics at kinetochores in Xenopus extract spindles: implications for spindle mechanics. *J. Cell Biol.* **162**, 377-382.

Maliga, Z., Kapoor, T. M. and Mitchison, T. J. (2002). Evidence that monastrol is an allosteric inhibitor of the mitotic kinesin Eg5. *Chem. Biol.* **9**, 989-996.

Manaka, A. and Sato, M. (2005). Synthesis of Aromatic Thioamide from Nitrile Without Handling of Gaseous Hydrogen Sulfide. *Synthetic Communications* **35**, 761-764.

Mayer, T. U., Kapoor, T. M., Haggarty, S. J., King, R. W., Schreiber, S. L. and Mitchison, T. J. (1999). Small molecule inhibitor of mitotic spindle bipolarity identified in a phenotype-based screen. *Science* **286**, 971-974.

McDonald, K. L., Edwards, M. K. and McIntosh, J. R. (1979). Cross-sectional structure of the central mitotic spindle of Diatoma vulgare. Evidence for specific interactions between antiparallel microtubules. *J. Cell Biol.* **83**, 443-461.

McIntosh, J. R. and Euteneuer, U. (1984). Tubulin hooks as probes for microtubule polarity: an analysis of the method and an evaluation of data on microtubule polarity in the mitotic spindle. *J. Cell Biol.* **98**, 525-533.

Merdes, A., Ramyar, K., Vechio, J. D. and Cleveland, D. W. (1996). A complex of NuMA and cytoplasmic dynein is essential for mitotic spindle assembly. *Cell* **87**, 447-458.

Mitchison, T. J., Maddox, P., Groen, A., Cameron, L., Perlman, Z., Ohi, R., Desai, A., Salmon, E. D. and Kapoor, T. M. (2004). Bipolarization and poleward flux correlate during Xenopus extract spindle assembly. *Mol. Biol. Cell* **15**, 5603-5615.

Mitchison, T. J., Maddox, P., Gaetz, J., Groen, A., Shirasu, M., Desai, A., Salmon, E. D. and Kapoor, T. M. (2005). Roles of polymerization dynamics, opposed motors, and a tensile element in governing the length of Xenopus extract meiotic spindles. *Mol. Biol. Cell* **16**, 3064-3076.

Miyamoto, D. T., Perlman, Z. E., Burbank, K. S., Groen, A. C. and Mitchison, T. J. (2004). The kinesin Eg5 drives poleward microtubule flux in Xenopus laevis egg extract spindles. *J. Cell Biol.* **167**, 813-818.

Murray, A. W. (1991). Cell cycle extracts. *Methods Cell Biol.* **36**, 581-605.

Parrish, C. A., Adams, N. D., Auger, K. R., Burgess, J. L., Carson, J. D., Chaudhari, A. M., Copeland, R. A., Diamond, M. A., Donatelli, C. A., Duffy, K. J. et al. (2007). Novel ATP-competitive kinesin spindle protein inhibitors. *J. Med. Chem.* **50**, 4939-4952.

Rickert, K. W., Schaber, M., Torrent, M., Neilson, L. A., Tasber, E. S., Garbaccio, R., Coleman, P. J., Harvey, D., Zhang, Y., Yang, Y. et al. (2008). Discovery and biochemical characterization of selective ATP competitive inhibitors of the human mitotic kinesin KSP. *Arch. Biochem. Biophys.* **469**, 220-231.

Salmon, E. D. and Begg, D. A. (1980). Functional implications of cold-stable microtubules in kinetochore fibers of insect spermatocytes during anaphase. *J. Cell Biol.* **85**, 853-865.

Sawin, K. E. and Mitchison, T. J. (1991). Poleward microtubule flux mitotic spindles assembled in vitro. *J. Cell Biol.* **112**, 941-954.

Sawin, K. E. and Mitchison, T. J. (1994). Microtubule flux in mitosis is independent of chromosomes, centrosomes, and antiparallel microtubules. *Mol. Biol. Cell* **5**, 217-226.

Sawin, K. E., LeGuellec, K., Philippe, M. and Mitchison, T. J. (1992). Mitotic spindle organization by a plus-end-directed microtubule motor. *Nature* **359**, 540-543.

Sharp, D. J., McDonald, K. L., Brown, H. M., Matthies, H. J., Walczak, C., Vale, R. D., Mitchison, T. J. and Scholey, J. M. (1999). The bipolar kinesin, KLP61F, cross-links microtubules within interpolar microtubule bundles of Drosophila embryonic mitotic spindles. *J. Cell Biol.* **144**, 125-138.

Thévenaz, P., Ruttimann, U. E. and Unser, M. (1998). A pyramid approach to subpixel registration based on intensity. *IEEE Trans. Image Proc.* **7**, 27-41.

Tirnauer, J. S., Canman, J. C., Salmon, E. D. and Mitchison, T. J. (2002a). EB1 targets to kinetochores with attached, polymerizing microtubules. *Mol. Biol. Cell* **13**, 4308-4316.

Tirnauer, J. S., Grego, S., Salmon, E. D. and Mitchison, T. J. (2002b). EB1-microtubule interactions in Xenopus egg extracts: role of EB1 in microtubule stabilization and mechanisms of targeting to microtubules. *Mol. Biol. Cell* **13**, 3614-3626.

Tirnauer, J. S., Salmon, E. D. and Mitchison, T. J. (2004). Microtubule plus-end dynamics in Xenopus egg extract spindles. *Mol. Biol. Cell* **15**, 1776-1784.

Verde, F., Berrez, J. M., Antony, C. and Karsenti, E. (1991). Taxol-induced microtubule asters in mitotic extracts of Xenopus eggs: requirement for phosphorylated factors and cytoplasmic dynein. *J. Cell Biol*. **112**, 1177-1187.

Walczak, C. E., Vernos, I., Mitchison, T. J., Karsenti, E. and Heald, R. (1998). A model for the proposed roles of different microtubule-based motor proteins in establishing spindle bipolarity. *Curr. Biol.* **8**, 903-913.

Waterman-Storer, C. M., Desai, A., Bulinski, J. C. and Salmon, E. D. (1998). Fluorescent speckle microscopy, a method to visualize the dynamics of protein assemblies in living cells. *Curr. Biol.* **8**, 1227-1230.

Wittmann, T. and Hyman, T. (1999). Recombinant p50/dynamitin as a tool to examine the role of dynactin in intracellular processes. *Methods Cell Biol.* **61**, 137-143.

Wittmann, T., Boleti, H., Antony, C., Karsenti, E. and Vernos, I. (1998). Localization of the kinesin-like protein Xklp2 to spindle poles requires a leucine zipper, a microtubule-associated protein, and dynein. *J. Cell Biol.* **143**, 673-685.

Wittmann, T., Wilm, M., Karsenti, E. and Vernos, I. (2000). TPX2, A novel xenopus MAP involved in spindle pole organization. *J. Cell Biol.* **149**, 1405-1418.

Wojcik, E. J., Dalrymple, N. A., Alford, S. R., Walker, R. A. and Kim, S. (2004). Disparity in allosteric interactions of monastrol with Eg5 in the presence of ADP and ATP: a difference FT-IR investigation. Biochemistry. **43**, 9939-9949.

Zheng, Y., Wong, M. L., Alberts, B. and Mitchison, T. (1995). Nucleation of microtubule assembly by a gamma-tubulin-containing ring complex. *Nature* **378**, 578-583.